Mon. Not. R. Astron. Soc. **000**, 1–?? (2013) Printed 11 February 2014 (MN LATEX style file v2.2)

Star-Disc-Binary Interactions in Protoplanetary Disc Systems and Primordial Spin-Orbit Misalignments

Dong Lai⋆
Center for Space Research, Department of Astronomy, Cornell University, Ithaca, NY 14853, USA

arXiv:1402.1907v1 [astro-ph.EP] 9 Feb 2014

11 February 2014

ABSTRACT

We study the interactions between a protostar and its circumstellar disc under the influence of an external binary companion to determine the evolution of the mutual misalignment between the stellar spin and the disc angular momentum axes. The gravitational torque on the disc from an inclined binary companion makes the disc precess around the binary axis, while the star-disc interaction torque due to the rotation-induced stellar quadrupole tends to make the stellar spin and the disc angular momentum axes precess around each other. A significant star-disc misalignment angle can be generated from a small initial value as the star-disc system evolves in time (e.g., with decreasing disc mass) such that the two precession frequencies cross each other. This "secular resonance" behaviour can be understood in a simple, geometric way from the precession dynamics of spin and disc angular momenta. We derive the general conditions for such resonance crossing to occur, and find that they can be satisfied for very reasonable protostar-disc-binary parameters. The evolution of star-disc inclination is also significantly affected by mass accretion from the disc onto the central star and by magnetic star-disc interaction torques, which can either promote or reduce star-disc misalignment, as well as by the possible damping of disc-binary inclination due to viscous dissipation of disc warps. In general, as long as the initial binary-disc inclination is not too small (greater than a few degrees), a variety of star-disc misalignment angles can be generated within the lifetimes of protoplanetary discs (~ 10 Myrs). We discuss the implications of our results for the observations of stellar spin orientations in binaries, for the alignments/misalignments of protostellar discs and debris discs relative to their host stars, and for the observed stellar obliquities in exoplanetary systems. In particular, if hot Jupiters are produced by the secular Lidov-Kozai effect induced by an external stellar companion present in the protostellar phase, then it is likely that "primordial" star-disc misalignments are already generated by the star-disc-binary interactions. Even for systems where the Kozai effect is suppressed, misaligned planets and hot Jupiters may still be produced during the protoplanetray disc phase.

Key words: planetary systems: protoplanetary discs – accretion, accretion discs – stars: magnetic fields – stars: rotation – binaries – stars: formation

1 INTRODUCTION

In the last few years, many exoplanetary systems containing hot Jupiters have been be found to have high stellar obliquities, i.e., large misalignment angles between the spin axis of the host star and the planetary orbital angular momentum axis (e.g., Hebrard et al. 2008; Winn et al. 2009,2010; Triaud et al. 2010; Moutou et al. 2011; Albrecht et al. 2012). This indicates that a large population of hot Jupiters are formed through high-eccentricity channels, either via dynamical planet-planet scatterings (Rasio & Ford 1996; Weidenschilling & Marzari 1996; Chatterjee et al. 2008; Juric & Tremaine 2008) or/and secular interactions between multiple planets, or Lidov-Kozai effect induced by a distant companion (e.g., Holman et al. 1997; Wu & Murray 2003; Fabrycky & Tremaine 2007; Wu et al. 2007; Nagasawa et al. 2008; Naoz et al. 2011,2102; Wu & Lithwick 2011; Katz et al. 2011). Alternatively, Rogers et al. (2012) suggested that the observed stellar obliquities may result from the torques

⋆ Email: dong@astro.cornell.edu

of varying directions deposited on the radiative stellar envelope by internally generated gravity waves.

The observed stellar obliquities may also contain contributions from (or be affected by) possible "primordial" misalignment between the the stellar spin and the protoplanetary disc. Several lines of evidence suggest that such primordial misalignment is possible:

(i) In the Solar system, all major planets lie in the same plane to within 2°, but this plane is inclined with respect to the solar rotational equator by 7°.

(ii) Solar-type main-sequence binaries with separations $\gtrsim 40$ AU often have rotation axis misaligned relative to the orbital angular momentum (Hale 1994).

(iii) Some binary young stellar objects (YSOs) are observed to have circumstellar discs that are misaligned with the binary orbital plane (e.g., Stapelfeldt et al. 1998,2003; Neuhauser et al. 2009). Also, several unresolved YSOs or pre-main sequence binaries have jet axes along different directions compared to the binary axes, suggesting misaligned discs (e.g., Davis, Mundt & Eislöffel 1994; Roccatagliata et al. 2011).

(iv) Recently, stellar obliquities in several multiplanet systems have been measured or constrained. While for some systems (Kepler-30, Sanchis-Ojeda et al. 2012; KOI-94 and Kepler-25, Albrecht et al. 2013, Hirano et al. 2012; Kepler-50 and Kepler-65, Chaplin et al. 2013), the stellar obliquities are consistent with zero (with typical error bars of order 10°), highly misaligned systems have also been found. In particular, Huber et al. (2013) used asteroseismology to measure a large stellar obliquity (40°-55°) for Kepler-56, a red giant star hosting two transiting coplanar planets with orbital period of 10.5 and 21 days. A companion in a wide orbit (as suggested by radial velocity data) may be responsible for the observed stellar obliquity; but it is possible that the companion was already present in the protoplanetary disc phase and produced a primordial misalignment. Also, there exists tentative evidence that the Kepler-9 system, containing three transiting, roughly coplanar planets (Holman et al. 2010), has a misaligned stellar spin (about 45°) with respect to the planetary orbit (Walkowicz & Basri 2013). Hirano et al. (2014) presented several other candidate misaligned multiplanet systems.

In contrast to the above, the current observational situation with debris disc systems seems different. In a number of debris disc systems, the stellar spin inclination (relative to the line of sight) $i_\star$ is similar to the debris disc inclination $i_{\rm disc}$, typically to within 10° (Watson et al. 2011; Greaves et al. 2013; Kennedy et al. 2013). While $i_\star \approx i_{\rm disc}$ does not necessarily imply alignment between the spin axis and the disc axis, statistically these observations do suggest that there is no significant star-disc misalignment in these systems.

There are several proposed mechanisms for tilting a star relative to its protoplanetary disc to produce primordial misalignment. Bate et al. (2010) suggested that in the chaotic star formation scenario, the accreting gas assembled onto a protoplanetary disc may have a varying direction of angular momentum, and thus the stellar spin direction can be different from the disc orientation at the later phase of accretion. Misalignment may also be produced when a protostellar system encounters another disc/envelope system with a different direction of rotation (Thies et al. 2011). Lai, Foucart & Lin (2011) showed that magnetic star-disc interaction produces a misalignment torque between the stellar spin and the disc axis (see also Lai 1999). However, this torque is of the same order of magnitude as the accretion torque, which tends to align the spin with the disc. Given the intrinsic complexity of the magnetic accretion physics, the net effect of the accretion and magnetic torques cannot be definitively determined at present: All one can say is that small or modest spin-disc misalignments may be produced in some systems; perhaps this is responsible for the 7° anomaly in the Solar system. To generate larger misalignments or retrograde discs require additional external perturbations (such as varying orientations of outer discs; see Foucart & Lai 2011).

Recently, Batygin (2012) suggested that the precession of a protoplanetary disc driven by the gravitational torque from an inclined binary companion can lead to misalignment between the stellar spin and the disc axis. This scenario is appealing since the same inclined binary companion is needed to make misaligned hot Jupiters through the secular Lidov-Kozai effect. Batygin & Adams (2013) further considered the coupling between the rotating central star and the precessing disc, and showed that significant misaligment between star and disc can be produced.

Since a large fraction of protostars are in binaries, the scenarios examined by Batygin (2012) and Batygin & Adams (2013) are of great interest and the mechanism of producing misalignment may be very robust. On the other hand, as noted above, the observational situation concerning spin-disc misalignment is confusing at present, with some protoplanetary discs showing misalignment, while many debris disc systems showing no significant misalignment.

In this paper we study the interactions between a protoplanetary disc, its host star and an external binary companion on an inclined orbit in order to understand the possibility and conditions of generating large spin-disc misalignments. Our approach to this problem is different from that of Batygin (2012) and Batygin & Adams (2013), and we also examine several additional physical effects not considered before. In particular, we model the star-disc-binary gravitational interactions directly using angular momentum equations (Sections 2-3). This allows us to describe the rotational dynamics of the system clearly in a physical way and see how different behaviours may arise under different conditions (i.e., different parameters of the system, such as disc size, rotation of the central star and the binary separation). We elucidate the significance of "secular resonance" in a geometric way (see Fig. 2 below) – such resonance plays an important role in producing large spin-disc misalignments. In Section 4, we study the effects of mass accretion and magnetic interaction between the star and the disc, including the possibility of magnetically driven spin-disc misalignment. We also briefly examine the effect of disc inclination damping (relative to the binary) associated with viscous dissipation of disc warping (Section 5). Overall, we find that all these effects can influence the final star-disc inclination significantly, and a variety of misalignment angles can be produced when a protostar disc is perturbed by a binary companion. In Section 6, we summarize the key physical effects and results (e.g., the conditions for resonance crossing), and discuss the implications of our findings for stellar binaries, protoplanetary/debris discs and the formation of misaligned planets.

2 GRAVITATIONAL TORQUES

2.1 Setup and Parameters of the Star-Disc-Binary System

We consider a protostellar system consisting of a primary star $M_\star$ surrounded by a disc and an external binary companion $M_{\rm b}$ (see Figure 1). To simplify the equations throughout the paper, we introduce dimensionless stellar mass, radius and rotation rate as

$$\bar{M}_\star = \frac{M_\star}{1\,M_\odot},\quad \bar{R}_\star = \frac{R_\star}{2R_\odot},\quad \bar{\Omega}_\star = \frac{\Omega_\star}{\sqrt{GM_\star/R_\star^3}}. \tag{1}$$

We also introduce dimensionless disc mass, inner radius and outer radius as

$$\bar{M}_{\rm d} = \frac{M_{\rm d}}{0.1M_\odot},\quad \bar{r}_{\rm in} = \frac{r_{\rm in}}{4R_\star},\quad \bar{r}_{\rm out} = \frac{r_{\rm out}}{50\,{\rm AU}}. \tag{2}$$

Note that

$$\Omega_\star = \left(\frac{2\pi}{3.3\,{\rm days}}\right)\left(\frac{\bar{\Omega}_\star}{0.1}\right)\left(\frac{\bar{M}_\star}{\bar{R}_\star^3}\right)^{1/2}. \tag{3}$$

The canonical value of $\bar{\Omega}_\star$ is 0.1, corresponding to rotation period $P_\star = 3.3$ days. The observed $P_\star$ for pre-main-sequence stars lies in the range between 1 and 10 days (e.g. Gallet & Bouvier 2013). For magnetic protostars, $r_{\rm in}$ is given by the magnetosphere radius, and $\Omega_\star$ and $r_{\rm in}$ are generally related such that $\Omega_\star$ is comparable to the disc Keplerian rotation rate at $r_{\rm in}$, i.e., the spin "fastness" parameter,

$$f_\star \equiv \frac{\Omega_\star}{\Omega_{\rm k}(r_{\rm in})} = 0.8\left(\frac{\bar{\Omega}_\star}{0.1}\right)\bar{r}_{\rm in}^{3/2}, \tag{4}$$

is of order unity (see Section 4.1).

The disc mass decreases in time due to accretion and mass outflow, with a lifetime of about 10 Myrs (see Section 3.3). The shape of the disc surface density profile also evolves in time. For simplicity, in this paper we assume a fixed power-law density profile (as adopted by Batygin & Adams 2013),

$$\Sigma = \Sigma_{\rm in}\frac{r_{\rm in}}{r}. \tag{5}$$

Thus the total disc mass is related to $\Sigma_{\rm in}$ via (assuming $r_{\rm out} \gg r_{\rm in}$)

$$M_{\rm d} \simeq 2\pi\Sigma_{\rm in} r_{\rm in} r_{\rm out}. \tag{6}$$

Throughout this paper, we mostly assume that the disc is flat (with negligible warp) and precesses like a rigid body. The exception in Section 6, where we consider the viscous damping of disc inclination due to disc warp. The reason the disc behaves as a rigid body is that different regions of the disc can communicate efficiently through bending waves and internal viscous stress (e.g., Papaloizou & Pringle 1983; Papaloizou & Lin 1995; Papaloizou & Terquem 1995; Ogilvie 1999,2006; Bate et al. 2000; Lubow & Ogilvie 2000), so that only a small disc warp is present in the disc (see Foucart & Lai 2011,2014 and references therein). Self gravity can also enhance this communication (Batygin 2012; Tremaine & Davis 2013).

The disc angular momentum vector is $\boldsymbol{L}_{\rm d} = L_{\rm d}\hat{\boldsymbol{L}}_{\rm d}$ (where $\hat{\boldsymbol{L}}_{\rm d}$ is the unit vector), with

$$L_{\rm d} \simeq \frac{2}{3}M_{\rm d}\sqrt{GM_\star r_{\rm out}}. \tag{7}$$

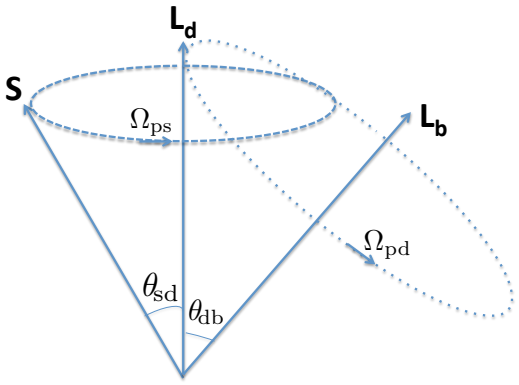

Figure 1. A sketch of the angular momentum axes of the star ($\boldsymbol{S}$), circumstellar disc ($\boldsymbol{L}_{\rm d}$) and external binary ($\boldsymbol{L}_{\rm b}$). The disc axis $\hat{\boldsymbol{L}}_{\rm d}$ precesses around the binary axis $\hat{\boldsymbol{L}}_{\rm b}$ at the rate $\Omega_{\rm pd}$, and the spin axis $\hat{\boldsymbol{S}}$ precesses around $\hat{\boldsymbol{L}}_{\rm d}$ at the rate $\Omega_{\rm ps}$ (assuming $L_{\rm b} \gg L_{\rm d} \gg S$).

The stellar spin angular momentum vector is $\boldsymbol{S} = S\hat{\boldsymbol{S}}$, with

$$S = k_\star M_\star R_\star^2 \Omega_\star. \tag{8}$$

where $k_\star \simeq 0.2$ for fully convective stars ($n = 1.5$ polytrope). The ratio of $L_{\rm d}$ and S is

$$\frac{L_{\rm d}}{S} = 244\left(\frac{M_{\rm d}}{0.1M_\star}\right)\left(\frac{0.2}{k_\star}\right)\left(\frac{0.1}{\bar{\Omega}_\star}\right)\left(\frac{\bar{r}_{\rm out}}{\bar{R}_\star}\right)^{1/2}. \tag{9}$$

The binary angular momentum is much larger, $L_{\rm b} \gg L_{\rm d}$, S.

2.2 Torques and Precession Rates

The rotation of the star gives rise to a quadrupole moment (the difference in moments of inertia around the two principal axes)

$$I_3 - I_1 = k_q M_\star R_\star^2 \bar{\Omega}_\star^2, \tag{10}$$

where $k_q \simeq 0.1$ for fully convective stars[1]. The gravitational torque on star from the disc is

$$\boldsymbol{T}_{\rm s} = -\int dM_{\rm d}\frac{3G(I_3 - I_1)}{2r^3}\cos\theta_{\rm sd}\,\hat{\boldsymbol{L}}_{\rm d}\times\hat{\boldsymbol{S}}, \tag{11}$$

where $dM_{\rm d} = 2\pi r\Sigma dr$. Using the density profile (5), we find

$$\boldsymbol{T}_{\rm s} = \Omega_{\rm ps}\hat{\boldsymbol{J}}_{\rm sd}\times\boldsymbol{S}. \tag{12}$$

Here $\boldsymbol{J}_{\rm sd} = J_{\rm sd}\hat{\boldsymbol{J}}_{\rm sd} = \boldsymbol{S} + \boldsymbol{L}_{\rm d}$ is the total angular momentum of the star-disc system, and $\Omega_{\rm ps}$ is the precession rate of the stellar spin around $\boldsymbol{J}_{\rm sd}$:

$$\Omega_{\rm ps} = -\frac{3GM_{\rm d}(I_3 - I_1)}{4r_{\rm in}^2 r_{\rm out}}\left(\frac{J_{\rm sd}}{L_{\rm d}S}\right)\cos\theta_{\rm sd}, \tag{13}$$

[1] For polytropic stellar models (with index n), k_q is approximately related to $k_\star$ via the relations $k_\star = 2\kappa_n/5$ and $k_q \simeq (\kappa_n^2/2)(1 - n/5)$ [see Lai et al. 1994, eq. (71)]. For $n = 0$ (incompressible fluid), $k_n = 1$ and these relations are exact. For $n = 1.5$ (fully convective stars), $\kappa_n \simeq 0.51$ (see Table 1 of Lai et al. 1993), which gives $k_\star \simeq 0.2$ and $k_q \simeq 0.09$.

where $\theta_{\rm sd}$ is the angle between $\boldsymbol{S}$ and $\boldsymbol{L}_{\rm d}$. Using equations (8) and (10), we find

$$\Omega_{\rm ps} = -\frac{3k_q}{4k_\star}\bar\Omega_\star \frac{M_{\rm d}}{M_\star}\frac{\sqrt{GM_\star R_\star^3}}{r_{\rm in}^2 r_{\rm out}}\left(\frac{J_{\rm sd}}{L_{\rm d}}\right)\cos\theta_{\rm sd}$$
$$= -4.86\times 10^{-5}\left(\frac{2k_q}{k_\star}\right)\left(\frac{M_{\rm d}}{0.1M_\star}\right)\left(\frac{\bar\Omega_\star}{0.1}\right)\frac{1}{\bar r_{\rm in}^2\bar r_{\rm out}}$$
$$\times\left(\frac{\bar M_\star}{\bar R_\star}\right)^{1/2}\left(\frac{J_{\rm sd}}{L_{\rm d}}\right)\cos\theta_{\rm sd}\left(\frac{2\pi}{\rm yr}\right). \quad (14)$$

Note that for $L_{\rm d}\gg S$, we have $J_{\rm sd}\simeq L_{\rm d}$ and $\Omega_{\rm ps}$ is simply the precession rate of $\boldsymbol{S}$ around $\boldsymbol{L}_{\rm d}$ (see Figure 1).

The torque on the disc from the external binary companion (mass $M_{\rm b}$ and separation $a_{\rm b}$) is

$$\boldsymbol{T}_{\rm d} = -\int dM_{\rm d}\frac{3GM_{\rm b}r^2}{4a_{\rm b}^3}\cos\theta_{\rm db}\,\hat{\boldsymbol{L}}_{\rm b}\times\hat{\boldsymbol{L}}_{\rm d}$$
$$= -\frac{GM_{\rm b}M_{\rm d}r_{\rm out}^2}{4a_{\rm b}^3}\cos\theta_{\rm db}\,\hat{\boldsymbol{L}}_{\rm b}\times\hat{\boldsymbol{L}}_{\rm d}$$
$$\equiv \Omega_{\rm pd}\hat{\boldsymbol{L}}_{\rm b}\times\boldsymbol{L}_{\rm d}, \quad (15)$$

where $\hat{\boldsymbol{L}}_{\rm b}$ is the unit vector along the binary angular momentum axis, and $\theta_{\rm db}$ is the angle between $\hat{\boldsymbol{L}}_{\rm d}$ and $\hat{\boldsymbol{L}}_{\rm b}$. The precession rate of the disc axis $\boldsymbol{L}_{\rm d}$ around the binary axis $\boldsymbol{L}_{\rm b}$ is then

$$\Omega_{\rm pd} = -\frac{3M_{\rm b}}{8M_\star}\left(\frac{GM_\star r_{\rm out}^3}{a_{\rm b}^6}\right)^{1/2}\cos\theta_{\rm db}$$
$$= -4.91\times 10^{-6}\left(\frac{M_{\rm b}}{M_\star}\right)\bar M_\star^{1/2}\bar r_{\rm out}^{3/2}\left(\frac{a_{\rm b}}{300\,{\rm AU}}\right)^{-3}$$
$$\times\cos\theta_{\rm db}\left(\frac{2\pi}{\rm yr}\right). \quad (16)$$

Finally, the binary companion also exerts a torque on the oblate star, given by

$$\boldsymbol{T}_{\rm s}' = -\frac{3GM_{\rm b}(I_3-I_1)}{2a_{\rm b}^3}(\hat{\boldsymbol{L}}_{\rm b}\cdot\hat{\boldsymbol{S}})\left(\hat{\boldsymbol{L}}_{\rm b}\times\hat{\boldsymbol{S}}\right). \quad (17)$$

But $|\boldsymbol{T}_{\rm s}'|$ is many orders of magnitude smaller than $|\boldsymbol{T}_{\rm s}|$, and will be neglected in this paper.

The ratio between $\Omega_{\rm ps}$ and $\Omega_{\rm pd}$ is of great importance for the spin evolution (Section 3) and is given by

$$\frac{\Omega_{\rm ps}}{\Omega_{\rm pd}} = 9.9\left(\frac{M_{\rm b}}{M_\star}\right)^{-1}\left(\frac{M_{\rm d}}{0.1M_\star}\right)\frac{1}{\bar r_{\rm out}^{5/2}\bar r_{\rm in}^2}\left(\frac{\bar\Omega_\star}{0.1}\right)\left(\frac{a_{\rm b}}{300\,{\rm AU}}\right)^3$$
$$\times\frac{1}{\bar R_\star^{1/2}}\left(\frac{2k_q}{k_\star}\right)\left(\frac{J_{\rm sd}}{L_{\rm d}}\right)\left(\frac{\cos\theta_{\rm sd}}{\cos\theta_{\rm db}}\right). \quad (18)$$

3 EVOLUTION OF SPIN DIRECTION DUE TO GRAVITATIONAL TORQUES

The gravitational torques discussed in Section 2 do not change the magnitudes of $\boldsymbol{L}_{\rm d}$ and $\boldsymbol{S}$. So the evolution equations of the spin and disc axes are

$$\frac{d\hat{\boldsymbol{S}}}{dt} = \Omega_{\rm ps}\hat{\boldsymbol{J}}_{\rm sd}\times\hat{\boldsymbol{S}}, \quad (19)$$
$$\frac{d\hat{\boldsymbol{L}}_{\rm d}}{dt} = \Omega_{\rm pd}\,\hat{\boldsymbol{L}}_{\rm b}\times\hat{\boldsymbol{L}}_{\rm d} + \Omega_{\rm ps}\hat{\boldsymbol{J}}_{\rm sd}\times\hat{\boldsymbol{L}}_{\rm d}. \quad (20)$$

Since $L_{\rm b}\gg L_{\rm d}$ and $L_{\rm b}\gg S$, we assume that $\hat{\boldsymbol{L}}_{\rm b}$ is a constant vector throughout this paper. Also, for $L_{\rm d}\gg S$ [see eq. (9)], $\boldsymbol{J}_{\rm sd}\simeq\boldsymbol{L}_{\rm d}$ and equations (19)-(20) reduce to

$$\frac{d\hat{\boldsymbol{S}}}{dt} \simeq \Omega_{\rm ps}\,\hat{\boldsymbol{L}}_{\rm d}\times\hat{\boldsymbol{S}}, \quad (21)$$
$$\frac{d\hat{\boldsymbol{L}}_{\rm d}}{dt} \simeq \Omega_{\rm pd}\,\hat{\boldsymbol{L}}_{\rm b}\times\hat{\boldsymbol{L}}_{\rm d} \qquad (\text{for } L_{\rm d}\gg S). \quad (22)$$

Our analysis below will be based on equations (21)-(22).

3.1 Limiting Cases: $|\Omega_{\rm ps}|\gg|\Omega_{\rm pd}|$ and $|\Omega_{\rm ps}|\ll|\Omega_{\rm pd}|$

While equations (21)-(22) can be integrated numerically in general, the solutions in two limiting cases are intuitively expected (see Section 3.2):

(i) For $|\Omega_{\rm ps}|\gg|\Omega_{\rm pd}|$, the vector $\hat{\boldsymbol{S}}$ rapidly processes around the slowly changing $\hat{\boldsymbol{L}}_{\rm d}$. Thus we expect $\hat{\boldsymbol{S}}$ to adiabatically follow $\hat{\boldsymbol{L}}_{\rm d}$ with $\theta_{\rm sd}\approx$ constant. The fractional variation of $\theta_{\rm sd}$ is of order $|\Omega_{\rm pd}|/|\Omega_{\rm ps}|$.

(ii) For $|\Omega_{\rm ps}|\ll|\Omega_{\rm pd}|$, the vector $\hat{\boldsymbol{S}}$ cannot keep up with the rapidly changing $\hat{\boldsymbol{L}}_{\rm d}$. In effect, $\hat{\boldsymbol{S}}$ will process around $\hat{\boldsymbol{L}}_{\rm b}$ with the rate $\Omega_{\rm ps}\cos\theta_{\rm db}$. That is, after averaging over time $P_{\rm pd}=2\pi/|\Omega_{\rm pd}|$, the spin axis satisfies the equation

$$\frac{d\langle\hat{\boldsymbol{S}}\rangle}{dt} \simeq \Omega_{\rm ps}\cos\theta_{\rm db}\,\hat{\boldsymbol{L}}_{\rm b}\times\langle\hat{\boldsymbol{S}}\rangle. \quad (23)$$

Thus, in this limit, we expect that the angle between $\hat{\boldsymbol{S}}$ and $\hat{\boldsymbol{L}}_{\rm b}$, $\theta_{\rm sb}\approx$ constant, with the fractional variation of order $|\Omega_{\rm ps}|/|\Omega_{\rm pd}|$.

3.2 Evolution Equations for $\theta_{\rm sd}$ and $\theta_{\rm sb}$

The statements in the last subsection can be justified from the evolution equations for $\theta_{\rm sd}$ and $\theta_{\rm sb}$, which we now derive from equations (21)-(22).

In the frame rotating around $\hat{\boldsymbol{L}}_{\rm b}$ at the rate $\Omega_{\rm pd}$, the vector $\hat{\boldsymbol{L}}_{\rm d}$ is constant, and the spin vector evolves according to

$$\left(\frac{d\hat{\boldsymbol{S}}}{dt}\right)_{\rm rot} \simeq \left(\Omega_{\rm ps}\,\hat{\boldsymbol{L}}_{\rm d} - \Omega_{\rm pd}\hat{\boldsymbol{L}}_{\rm b}\right)\times\hat{\boldsymbol{S}}. \quad (24)$$

Thus, in this rotating frame, $\hat{\boldsymbol{S}}$ processes around the axis $\hat{\boldsymbol{L}}_e$ with the rate Ω_e, where

$$\Omega_{\rm e}\hat{\boldsymbol{L}}_{\rm e} = \Omega_{\rm ps}\hat{\boldsymbol{L}}_{\rm d} - \Omega_{\rm pd}\hat{\boldsymbol{L}}_{\rm b}, \quad (25)$$
$$\Omega_{\rm e} = -\left(\Omega_{\rm ps}^2+\Omega_{\rm pd}^2-2\Omega_{\rm ps}\Omega_{\rm pd}\cos\theta_{\rm db}\right)^{1/2}. \quad (26)$$

It is now easy to see the results stated in Section 3.1 (see Fig. 2): (i) For $|\Omega_{\rm ps}|\gg|\Omega_{\rm pd}|$, we have $\hat{\boldsymbol{L}}_{\rm e}\simeq\hat{\boldsymbol{L}}_{\rm d}$, and $\hat{\boldsymbol{S}}$ precesses around $\hat{\boldsymbol{L}}_{\rm d}$ with constant $\theta_{\rm sd}$. (ii) For $|\Omega_{\rm ps}|\ll|\Omega_{\rm pd}|$, we have $\hat{\boldsymbol{L}}_{\rm e}\simeq\hat{\boldsymbol{L}}_{\rm b}$ (with a possible sign difference), and $\hat{\boldsymbol{S}}$ precesses around $\hat{\boldsymbol{L}}_{\rm b}$ with constant $\theta_{\rm sb}$.

If $\Omega_{\rm ps}$ and $\Omega_{\rm pd}$ do not vary in time, or more generally, if the rate of change of $|\Omega_e|\hat{\boldsymbol{L}}_e$ is much less than $|\Omega_e|$, then equation (24) can be easily solved. Suppose at $t=0$, the vector $\hat{\boldsymbol{S}}$ lies in the same plane as $\hat{\boldsymbol{L}}_{\rm d}$ and $\hat{\boldsymbol{L}}_{\rm b}$ (see Fig. 2). Define the basis vectors $\hat{\mathbf{e}}_3=\hat{\boldsymbol{L}}_{\rm e}$, $\hat{\mathbf{e}}_2\propto\hat{\boldsymbol{L}}_{\rm b}\times\hat{\boldsymbol{L}}_{\rm d}$, and $\hat{\mathbf{e}}_1=\hat{\mathbf{e}}_2\times\hat{\mathbf{e}}_3$. Then at $t>0$, the components of $\hat{\boldsymbol{S}}$ along these bases are

$$\hat S_1 \simeq -\sin\theta_{\rm se}\cos\Phi_{\rm se}(t), \quad (27)$$
$$\hat S_2 \simeq -\sin\theta_{\rm se}\sin\Phi_{\rm se}(t), \quad (28)$$
$$\hat S_3 \simeq \cos\theta_{\rm se}, \quad (29)$$

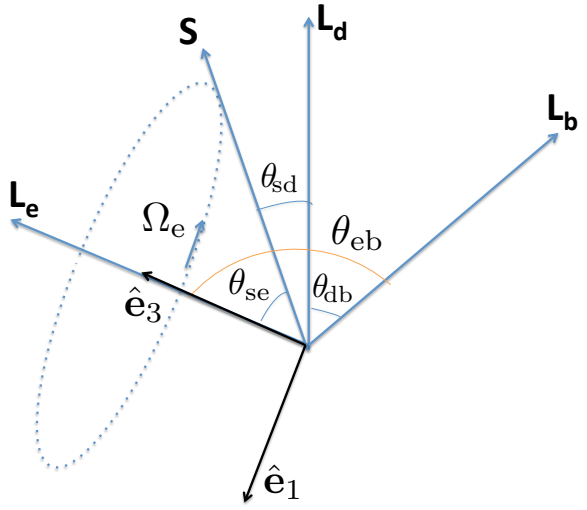

Figure 2. A sketch of the angular momentum axes of the star ($\boldsymbol{S}$), circumstellar disc ($\boldsymbol{L}_{\rm d}$), and external binary ($\boldsymbol{L}_{\rm b}$). In the frame rotating around $\boldsymbol{L}_{\rm b}$ with rate $\Omega_{\rm pd}$ (see Fig. 1), the vector $\boldsymbol{L}_{\rm d}$ is constant (assuming $L_{\rm d} \gg S$), and the stellar spin $\boldsymbol{S}$ precesses around the vector $\hat{\boldsymbol{L}}_{\rm e}$ [defined by eq. (25)] at the rate $\Omega_{\rm e}$. For $|\Omega_{\rm ps}| \gg |\Omega_{\rm pd}|$, we have $\hat{\boldsymbol{L}}_{\rm e} \simeq \hat{\boldsymbol{L}}_{\rm d}$, thus $\theta_{\rm sd} \simeq$ constant. For $|\Omega_{\rm ps}| \ll |\Omega_{\rm pd}|$, we have $\hat{\boldsymbol{L}}_{\rm e} \simeq \hat{\boldsymbol{L}}_{\rm b}$, thus $\theta_{\rm sb} \simeq$ constant. For $\Omega_{\rm ps} = \Omega_{\rm pd}$ ("secular resonance"), $\hat{\boldsymbol{L}}_{\rm e} \propto \hat{\boldsymbol{L}}_{\rm d} - \hat{\boldsymbol{L}}_{\rm b}$ deviates significantly from $\hat{\boldsymbol{L}}_{\rm d}$ even for small initial $\theta_{\rm sd}$ and $\theta_{\rm db}$; thus a large $\theta_{\rm sd}$ can be produced as $\hat{\boldsymbol{S}}$ precesses around $\hat{\boldsymbol{L}}_{\rm e}$. The Cartesian basis $(\hat{\mathbf{e}}_1, \hat{\mathbf{e}}_2, \hat{\mathbf{e}}_3)$ is used in eqs. (27)-(29).

where

$$\Phi_{\rm se}(t) = \int_0^t dt\, \Omega_{\rm e}, \tag{30}$$

and $\theta_{\rm se}$ is the angle between $\hat{\boldsymbol{S}}$ and $\hat{\boldsymbol{L}}_{\rm e}$, and is determined by its value at $t = 0$, i.e., $\theta_{\rm se} = \theta_{\rm se,0} = \theta_{\rm eb} - \theta_{\rm sd,0} - \theta_{\rm db}$, with $\theta_{\rm eb}$ the angle bewteen $\hat{\boldsymbol{L}}_e$ and $\hat{\boldsymbol{L}}_{\rm b}$.

From equations (21)-(22), we have

$$\begin{aligned} \frac{d}{dt}\cos\theta_{\rm sd} &\simeq \hat{\boldsymbol{S}} \cdot \left(\Omega_{\rm pd}\, \hat{\boldsymbol{L}}_{\rm b} \times \hat{\boldsymbol{L}}_{\rm d}\right) \\ &\simeq -\Omega_{\rm pd} \sin\theta_{\rm db} \sin\theta_{\rm se} \sin\Phi_{\rm se}(t), \end{aligned} \tag{31}$$

where in the second equality we have used equation (28). Similarly, from equation (21), we have

$$\begin{aligned} \frac{d}{dt}\cos\theta_{\rm sb} &\simeq \hat{\boldsymbol{L}}_{\rm b} \cdot \left(\Omega_{\rm ps}\, \hat{\boldsymbol{L}}_{\rm d} \times \hat{\boldsymbol{S}}\right) = \Omega_{\rm ps} \hat{\boldsymbol{S}} \cdot \left(\hat{\boldsymbol{L}}_{\rm b} \times \hat{\boldsymbol{L}}_{\rm d}\right) \\ &\simeq -\Omega_{\rm ps} \sin\theta_{\rm db} \sin\theta_{\rm se} \sin\Phi_{\rm se}(t). \end{aligned} \tag{32}$$

For constant $\Omega_{\rm pd}$ and $\Omega_{\rm ps}$, equations (31) -(32) give

$$\cos\theta_{\rm sd} - \cos\theta_{\rm sd,0} \simeq \frac{\Omega_{\rm pd}}{\Omega_e} \sin\theta_{\rm db} \sin\theta_{\rm se} \left(\cos\Omega_e t - 1\right), \tag{33}$$

$$\cos\theta_{\rm sb} - \cos\theta_{\rm sb,0} \simeq \frac{\Omega_{\rm ps}}{\Omega_e} \sin\theta_{\rm db} \sin\theta_{\rm se} \left(\cos\Omega_e t - 1\right). \tag{34}$$

With these two equations, the limiting cases of Section 3.1 can be understood precisely:

(i) For $|\Omega_{\rm ps}| \gg |\Omega_{\rm pd}|$, we have $\hat{\boldsymbol{L}}_{\rm e} \simeq \hat{\boldsymbol{L}}_{\rm d}$, $|\Omega_e| \simeq |\Omega_{\rm ps}|$ and $|\theta_{\rm se}| \simeq |\theta_{\rm sd}|$, so $\theta_{\rm sd} \approx$ constant, with variation $\Delta\theta_{\rm sd} \sim (\Omega_{\rm pd}/\Omega_{\rm ps}) \sin\theta_{\rm db}$.

(ii) For $|\Omega_{\rm ps}| \ll |\Omega_{\rm pd}|$, $\hat{\boldsymbol{L}}_{\rm e} \simeq \hat{\boldsymbol{L}}_{\rm b}$, $|\Omega_e| \simeq |\Omega_{\rm pd}|$ and $|\theta_{\rm se}| \simeq |\theta_{\rm sb}|$, so $\theta_{\rm sb} \approx$ constant, with variation $\Delta\theta_{\rm sb} \sim (\Omega_{\rm ps}/\Omega_{\rm pd}) \sin\theta_{\rm db}$.

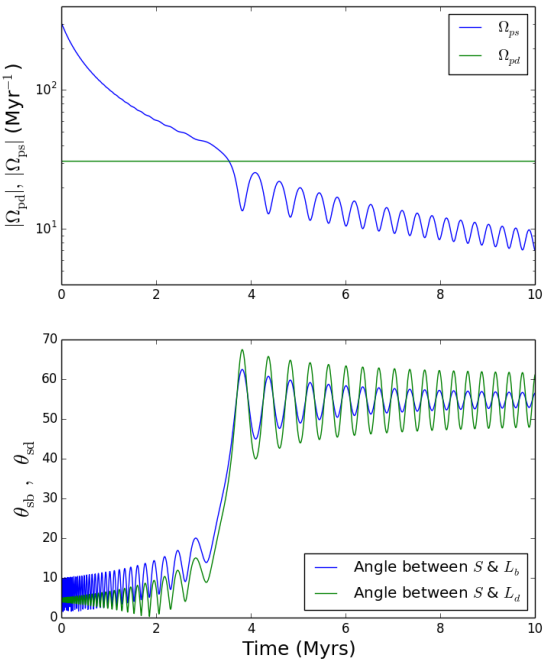

Figure 3. Evolution of the stellar spin direction due to interactions with circumstellar disc and external binary companion. The upper panel shows the disc precession rate $|\Omega_{\rm pd}|$ and the stellar precession rate $|\Omega_{\rm ps}|$, while the lower panel shows the spin-disc angle $\theta_{\rm sd}$ and spin-binary angle $\theta_{\rm sb}$. The initial values for various angles are: disc-binary $\theta_{\rm db} = 5°$ (which is constant in time when $L_{\rm d} \gg S$), spin-disc $\theta_{\rm sd} = 5°$, spin-binary $\theta_{\rm sb} = 10°$. The initial disc mass is $M_{\rm d0} = 0.1 M_\star$. The other parameters are fixed at their canonical values shown in equations (14) and (16): $2k_q/k_\star = 1$, $\bar{\Omega}_\star = 0.1$, $\bar{r}_{\rm in} = \bar{r}_{\rm out} = 1$, $\bar{M}_\star = \bar{R}_\star = 1$, $M_{\rm b} = M_\star$, and $a_{\rm b} = 300$ AU.

3.3 General Cases: Evolving Discs

We now consider the cases when the parameters of disc-star system evolve in time. In general, the stellar radius and spin can change, as well as the disc inner and outer radii, all on timescales of order a few Myrs. Here, for concreteness, we only consider the evolution of the disc mass $M_{\rm d}$, which directly affects the spin precession rate $\Omega_{\rm ps}$. In this section we neglect mass accretion and other effects on the stellar spin (see Section 4), and we also neglect any direct effect of changing disc mass on the disc orientation. We assume that the disc mass evolves in time according to (Batygin & Adams 2013)

$$M_{\rm d} = \frac{M_{\rm d0}}{1 + t/\tau}. \tag{35}$$

For our canonical parameters, we choose $M_{\rm d0} = 0.1 M_\odot$ and $\tau = 0.5$ Myrs.

Figures 3-6 show the evolution of the stellar spin direction relative to the disc axis and to the binary axis for different initial disc-binary angle $\theta_{\rm db}$ ($= 5°, 30°, 60°, 80°$). Note that this angle does not change in time when $L_{\rm b} \gg L_{\rm d} \gg S$.

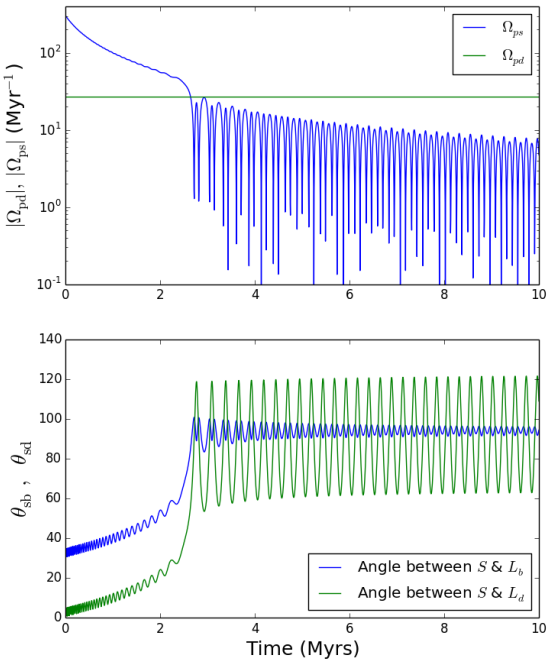

Figure 4. Same as Fig. 3, except for the initial disc-binary angle $\theta_{\rm db} = 30^\circ$ and spin-binary angle $\theta_{\rm sb} = 35^\circ$.

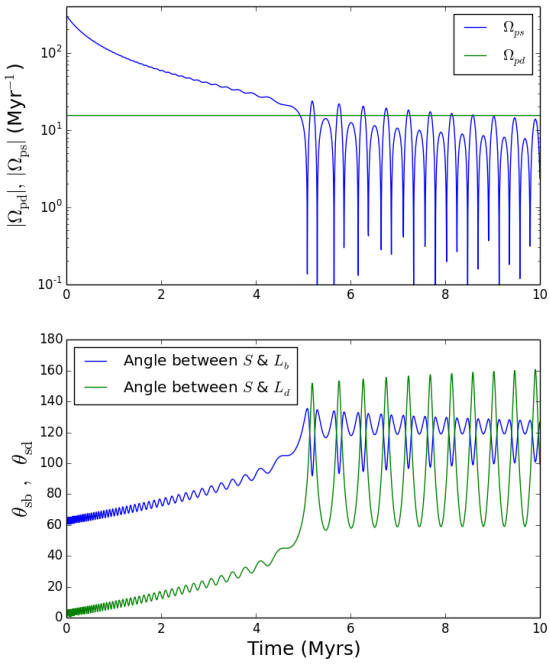

Figure 5. Same as Fig. 3, except for the initial disc-binary angle $\theta_{\rm db} = 60^\circ$ and spin-binary angle $\theta_{\rm sb} = 65^\circ$.

The initial spin-disc angle $\theta_{\rm sd}$ is fixed at 5°, and $\hat{\boldsymbol{S}}, \hat{\boldsymbol{L}}_{\rm d}, \hat{\boldsymbol{L}}_{\rm b}$ lie in the same plane at $t = 0$. The other parameters assume their canonical values made explicit in equations (14) and (16): $M_\star = 1\,M_\odot$, $R_\star = 2R_\odot$, $\bar{\Omega}_\star = 0.1$, $k_\star = 2k_q$, $r_{\rm in} = 4R_\star$, $r_{\rm out} = 50$ AU, $M_{\rm b} = M_\star$ and $a_{\rm b} = 300$ AU. We see that at early time, when $M_{\rm d}$ is large, the inequality $|\Omega_{\rm ps}| \gg |\Omega_{\rm pd}|$ is satisfied, and $\hat{\boldsymbol{S}}$ adiabatically tracks $\hat{\boldsymbol{L}}_{\rm d}$, with $\theta_{\rm sd}$ approximately holding constant. Unless $|\cos\theta_{\rm db}|$ is too small (see Fig. 6 for the case of $\theta_{\rm db} = 80^\circ$), which implies very small $|\Omega_{\rm pd}|$, the system will evolve to the regime $|\Omega_{\rm pd}| \gtrsim |\Omega_{\rm ps}|$ within 10 Myrs, and large $\theta_{\rm sd}$ can be developed. As expected (see Section 3.1), when $|\Omega_{\rm pd}| \gg |\Omega_{\rm ps}|$, the stellar spin effectively precesses around the binary axis $\hat{\boldsymbol{L}}_{\rm b}$, with $\theta_{\rm sb}$ approximately constant. The detailed evolution of the spin direction is complicated by the fact that $\Omega_{\rm ps}$ crosses zero at $\theta_{\rm sd} = 90^\circ$.

The evolution of spin direction depends sensitively on the binary separation $a_{\rm b}$. Figure 7 depicts some examples for $a_{\rm b} = 400$ and 600 AU (the corresponding case of $a_{\rm b} = 300$ AU is shown in Fig. 4). Obviously, for distant companion ($a_{\rm b} \gtrsim 10^3$ AU), the condition $|\Omega_{\rm ps}| \gg |\Omega_{\rm pd}|$ is always satisfied, and the stellar spin can adiabatically follow the slowly-precessing disc and the angle $\theta_{\rm sd}$ retains its initial value.

3.4 Understanding "Secular Resonance"

The fact that significant change in $\theta_{\rm sd}$ occurs when $|\Omega_{\rm ps}| \sim |\Omega_{\rm pd}|$ is a signature of "secular resonance" (Batygin & Adams 2013). The significance of this resonance can be understood geometrically from Fig. 2: For $\Omega_{\rm ps} = \Omega_{\rm pd}$, the vector $\hat{\boldsymbol{L}}_{\rm e} \propto \hat{\boldsymbol{L}}_{\rm d} - \hat{\boldsymbol{L}}_{\rm b}$ deviates significantly from $\hat{\boldsymbol{L}}_{\rm d}$ even for small initial $\theta_{\rm sd}$ and $\theta_{\rm db}$; thus $\theta_{\rm sd}$ oscillates from its initial (possibly small) value to a very large value as $\hat{\boldsymbol{S}}$ precesses around $\hat{\boldsymbol{L}}_{\rm e}$. In the cases where the ratio $\Omega_{\rm ps}/\Omega_{\rm pd}$ varies in time and transitions from above unity to below unity (as in the examples depicted in Section 3.3), this oscillation of $\theta_{\rm sd}$ is incomplete, but a large value of $\theta_{\rm sd}$ can be generated as the system crosses the resonance.

The actual change of $\theta_{\rm sd}$ associated with resonance crossing depends on how fast the system evolves through the resonance, or in the examples of Section 3.3, how fast the disc mass decreases. Consider two limiting cases:

(i) If $|\Omega_{\rm ps}/\Omega_{\rm pd}|$ evolves from $\gg 1$ to $\ll 1$ very slowly, at an rate smaller than $|\Omega_e|$ for all times, i.e., if $|\dot{\Omega}_e/\Omega_e| \ll |\Omega_e|$, then $\hat{\boldsymbol{S}}$ will adiabatically precess around $\hat{\boldsymbol{L}}_{\rm e}$ with a constant $\theta_{\rm se}$. Thus, if the initial spin-disc angle is $\theta_{\rm sd,0}$, we have $\theta_{\rm se} = \theta_{\rm sd,0}$ (since $\hat{\boldsymbol{L}}_{\rm e} = \hat{\boldsymbol{L}}_{\rm d}$ initially); in the end (when $|\Omega_{\rm ps}/\Omega_{\rm pd}| \ll 1$), we have $\hat{\boldsymbol{L}}_{\rm e} = \hat{\boldsymbol{L}}_{\rm b}$ and $\theta_{\rm sb} = \theta_{\rm se} = \theta_{\rm sd,0}$, with $\theta_{\rm sd}$ oscillating between $|\theta_{\rm sd,0} - \theta_{\rm db}|$ and $\theta_{\rm sd,0} + \theta_{\rm db}$.

(ii) If $|\Omega_{\rm ps}/\Omega_{\rm pd}|$ changes from $\gg 1$ to $\ll 1$ "suddenly" at time $t = t_c$, at a rate much larger than $|\Omega_{\rm e}|$, then $\hat{\boldsymbol{S}}$ will suddenly transition from precessing around $\hat{\boldsymbol{L}}_{\rm d}$ to precessing around $\hat{\boldsymbol{L}}_{\rm b}$. The final $\theta_{\rm sb}$ is simply given by its value just before the transition. Depending on the precssion phase at the transition, this final $\theta_{\rm sb,f}$ will range from $|\theta_{\rm sd,0} - \theta_{\rm db}|$ to $\theta_{\rm sd,0} + \theta_{\rm db}$, with $\theta_{\rm sd}$ oscillating between $|\theta_{\rm sb,f} - \theta_{\rm db}|$ and $\theta_{\rm sb,f} + \theta_{\rm db}$.

In the cases depicted in Section 3.3, neither the "slow evolution" or the "sudden evolution" limit applies in general, since the disc evolution time ($\sim$ Myrs) is comparable to the disc/star precession times for typical disc/star/binary parameters [from eq. (26), we see that $|\Omega_e|$ reaches its minimum value $|\Omega_{\rm pd}|\sin\theta_{\rm db}$ when $|\Omega_{\rm ps}| = |\Omega_{\rm pd}\cos\theta_{\rm db}|$]. Thus the evolution of $\theta_{\rm sd}$ or $\theta_{\rm sb}$ across the resonance cannot be predicted in a simple analytical manner. Nevertheless the

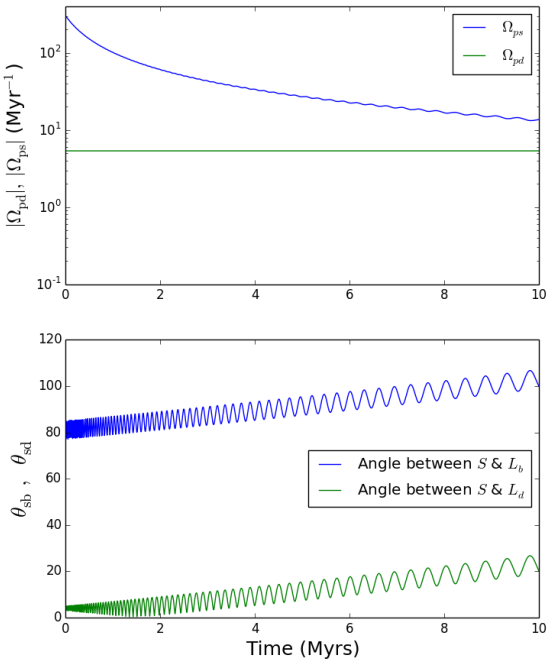

Figure 6. Same as Fig. 3, except for the initial disc-binary angle $\theta_{\rm db} = 80°$ and spin-binary angle $\theta_{\rm sb} = 85°$.

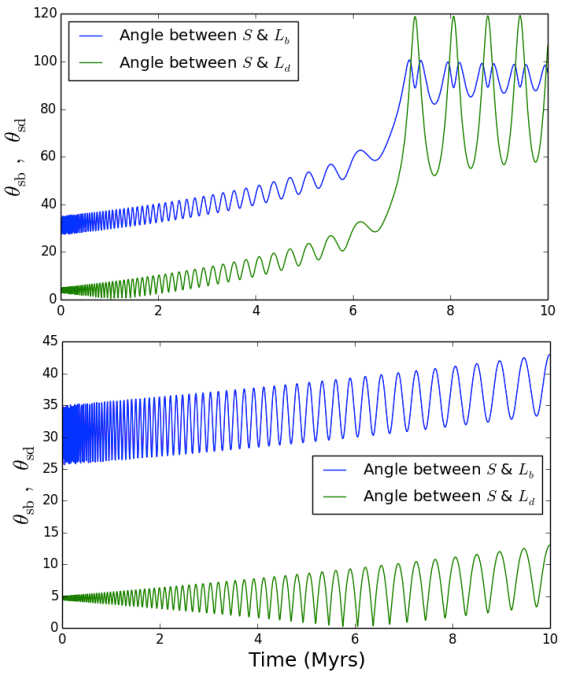

Figure 7. Evolution of the stellar spin direction due to interactions with circumstellar disc and external binary companion. The parameters are the same as in Fig. 4 (i.e., the initial $\theta_{\rm db} = 30°$ and $\theta_{\rm sb} = 35°$), except $a_{\rm b} = 400$ AU (upper panel) and $a_{\rm b} = 600$ AU (lower panel).

discussion above and Fig. 2 capture the essential features of the resonance transition.

4 ACCRETION AND MAGNETIC TORQUES

In the previous sections we included only gravitational torques in the spin-disc evolution. Here we consider the effects of mass accretion and magnetic torques on the star. Protostars are known to have magnetic fields of order 10^3 G, and magnetic interactions between the star and the disc play an important role in determining the stellar spin evolution – there is a large literature on this subject; see, e.g., Bouvier et al. (2007), Lai (2014), Romanova et al. (2014) for recent reviews.

4.1 Model for Spin and Disc Evolution

The vast majority of studies of magnetic star - disc interactions assume that the stellar spin axis is aligned with the disc axis. Lai et al. (2011) presented a model for the evolution of protostellar spin for misaligned discs, including accretion, wind and magnetic effects. Combining equation (15) of Lai et al. (2011) with the gravitational torque discussed in Section 2, we have

$$\frac{d\boldsymbol{S}}{dt} = \lambda \mathcal{N}_0 \hat{\boldsymbol{L}}_{\rm d} - \mathcal{N}_{\rm s}\hat{\boldsymbol{S}} + \mathcal{N}_0\, \bar{n}_w \cos\theta_{\rm sd}\, \hat{\boldsymbol{L}}_{\rm d} \times (\hat{\boldsymbol{S}} \times \hat{\boldsymbol{L}}_{\rm d}) + \mathcal{N}_0\, \bar{n}_p \cos\theta_{\rm sd} \hat{\boldsymbol{S}} \times \hat{\boldsymbol{L}}_{\rm d} + \Omega_{\rm ps} \hat{\boldsymbol{J}}_{\rm sd} \times \boldsymbol{S}, \quad (36)$$

where

$$\mathcal{N}_0 = \dot{M}\sqrt{GM_\star r_{\rm in}}, \quad (37)$$

is the standard accretion torque, with $\dot{M}$ the mass accretion rate onto the star.

The first term on the right-hand side of equation (36) represents the total torque in the direction of $\hat{\boldsymbol{L}}_{\rm d}$; it includes the accretion torque carried by the gas onto the star, the magnetic braking torque associated with the disc-star linkage, as well as any angular momentum carried away by winds/outflows from the magnetosphere boundary. While the details are complex, all these contributions tend to make $\lambda < 1$, as suggested by numerical simulations and semi-analytic works (see Romanova et al. 2014, Lai 2014 and references therein). The second term in equation (36) represents the spindown torque along the $\hat{\boldsymbol{S}}$ direction; for example, it could include torques associated with winds/jets from the open field line region of the star.

The third and fourth terms in equation (36) represent the magnetic misalignment and precessional torques, whose physical origins have been discussed in detail in Lai et al. (2011) (see also Lai 1999). The dimensionless parameters $\bar{n}_w$ and $\bar{n}_p$ depend on the details of the physics of magnetosphere-disc interaction, and are expected to be of order unity. The last term in equation (36) is the gravitational torque from the disc, as calculated in Section 2.

Multiplying equation (36) by $\hat{\boldsymbol{S}}$ (dot product), we find that the magnitude of $\boldsymbol{S}$ evolves according to

$$\frac{d\,S}{dt} = \mathcal{N}_0 \cos\theta_{\rm sd}\left(\lambda + \bar{n}_w \sin^2\theta_{\rm sd}\right) - \mathcal{N}_{\rm s}. \quad (38)$$

Obviously, without a detailed knowledge of λ (characterizing the torques associated with accretion and magnetic

star-disc linkage) and $\mathcal{N}_{\rm s}$ (characterizing stellar outflows), it it not possible to follow the evolution of S in quantitative details. For the reminder of this paper, we will bypass this problem by assuming that the stellar spin reaches the equilibrium value, such that $\Omega_\star$ is comparable to the disc Keplerian rotation rate at $r_{\rm in}$. For our canonical star-disc parameters [see eqs. (1)-(2)], the spin "fastness parameter" $f_\star$ is given by equation (4). Various analytical and numerical studies for aligned ($\hat{\boldsymbol{L}}_{\rm d}=\hat{\boldsymbol{S}}$) magnetic star-disc systems suggest that $f_\star$ is in the range of 0.5-1 (e.g., Ghosh & Lamb 1979; Königl 1991; Shu et al. 1994; Long et al. 2005 and references therein).

Combining equations (36) and (38), we find the stellar spin direction evolves according to the equation

$$\frac{d\hat{\boldsymbol{S}}}{dt}=\omega_0\left(\lambda-\bar{n}_w\cos^2\theta_{\rm sd}\right)\left(\hat{\boldsymbol{L}}_{\rm d}-\cos\theta_{\rm sd}\hat{\boldsymbol{S}}\right) +\Omega_{\rm ps}^{(m)}\hat{\boldsymbol{J}}_{\rm sd}\times\hat{\boldsymbol{S}}+\Omega_{\rm ps}\hat{\boldsymbol{J}}_{\rm sd}\times\hat{\boldsymbol{S}}, \quad (39)$$

where

$$\omega_0\equiv\frac{\mathcal{N}_0}{S}=\frac{\bar{r}_{\rm in}^{1/2}}{\bar{M}_\star}\left(\frac{0.2}{k_\star}\right)\left(\frac{0.1}{\bar{\Omega}_\star}\right)\left(\frac{\dot{M}}{10^{-8}M_\odot/{\rm yr}}\right)\ {\rm Myr}^{-1} \quad (40)$$

is the inverse of the characteristic spinup time due to accretion, and

$$\Omega_{\rm ps}^{(m)}=-\omega_0\,\bar{n}_p\,\cos\theta_{\rm sd}\left(\frac{J_{\rm sd}}{L_{\rm d}}\right) \quad (41)$$

is the stellar precession rate due to the magnetic torque.

The angular momentum equation for the disc can be written as

$$\frac{d\boldsymbol{L}_{\rm d}}{dt}=-\mathcal{N}_{\rm d}\hat{\boldsymbol{L}}_{\rm d}-\mathcal{N}_0\,\bar{n}_w\cos\theta_{\rm sd}\,\hat{\boldsymbol{L}}_{\rm d}\times(\hat{\boldsymbol{S}}\times\hat{\boldsymbol{L}}_{\rm d}) -\mathcal{N}_0\,\bar{n}_p\cos\theta_{\rm sd}\hat{\boldsymbol{S}}\times\hat{\boldsymbol{L}}_{\rm d}+\Omega_{\rm ps}\hat{\boldsymbol{J}}_{\rm sd}\times\boldsymbol{L}_{\rm d} +\Omega_{\rm pd}\,\hat{\boldsymbol{L}}_{\rm b}\times\boldsymbol{L}_{\rm d}. \quad (42)$$

Here, the first term on the on the right-hand side represents various disc torques (e.g., associated with angular momentum loss due to mass accretion or disc winds/outflows) that are aligned with $\hat{\boldsymbol{L}}_{\rm d}$, the second and third terms are the magnetic misalignment and precessional torques, and the fourth and fifth terms are the gravitational torques from the star and from the external binary (see Section 2). The magnitude of disc angular momentum evolves as $dL_{\rm d}/dt=-\mathcal{N}_{\rm d}$, and the direction vector $\hat{\boldsymbol{L}}_{\rm d}$ satisfies the equation

$$\frac{d\hat{\boldsymbol{L}}_{\rm d}}{dt}=-\left(\frac{\mathcal{N}_0}{L_{\rm d}}\right)\bar{n}_w\cos\theta_{\rm sd}\left(\hat{\boldsymbol{S}}-\cos\theta_{\rm sd}\,\hat{\boldsymbol{L}}_{\rm d}\right) +\Omega_{\rm ps}^{(m)}\hat{\boldsymbol{J}}_{\rm sd}\times\hat{\boldsymbol{L}}_{\rm d}+\Omega_{\rm ps}\hat{\boldsymbol{J}}_{\rm sd}\times\hat{\boldsymbol{L}}_{\rm d} +\Omega_{\rm pd}\,\hat{\boldsymbol{L}}_{\rm b}\times\hat{\boldsymbol{L}}_{\rm d} \quad (43)$$

Combining equations (39) and (43), we find

$$\frac{d\cos\theta_{\rm sd}}{dt}=\omega_0\sin^2\theta_{\rm sd}\left[\lambda-\bar{n}_w\cos\theta_{\rm sd}\left(\cos\theta_{\rm sd}+\frac{S}{L_{\rm d}}\right)\right] +\Omega_{\rm pd}\hat{\boldsymbol{S}}\cdot\left(\hat{\boldsymbol{L}}_{\rm b}\times\hat{\boldsymbol{L}}_{\rm d}\right). \quad (44)$$

Ignoring the term associated with disc precession [the second line of eq. (44)], the above equation generalizes the result of Lai et al. (2011), where large discs with $L_{\rm d}\gg S$ were considered. The combined effects of accretion and magnetic torque on the evolution of $\theta_{\rm sd}$ (again ignoring disc precession) depend on the ratio $\lambda/\bar{n}_w$ (assuming $S/L_d\ll1$ for simplicity; see Lai et al. 2011, especially their Fig. 4):

(i) For $\lambda/\bar{n}_w>1$: Regardless of the value of $\theta_{\rm sd}$, the spin axis $\hat{\boldsymbol{S}}$ is always driven towards alignment with $\hat{\boldsymbol{L}}_{\rm d}$ (i.e., $\theta_{\rm sd}$ always decreases).

(ii) For $\lambda/\bar{n}_w<1$: There are two "equilibrium" states, $\theta_{\rm sd+}$ and $\theta_{\rm sd-}$, given by

$$\cos\theta_{\rm sd\pm}=\pm\sqrt{\lambda/\bar{n}_w}, \quad (45)$$

one of which ($\theta_{\rm sd+}<90^\circ$) is stable and the other ($\theta_{\rm sd-}>90^\circ$) unstable. Thus, $\theta_{\rm sd}$ increases toward $\theta_{\rm sd+}$ for $\theta_{\rm sd}<\theta_{\rm sd+}$, decreases toward $\theta_{\rm sd+}$ for $\theta_{\rm sd+}<\theta_{\rm sd}<\theta_{\rm sd-}$, and increases toward 180° for $\theta_{\rm sd}>\theta_{\rm sd-}$.

Although the values of λ and n_w are difficult to evaluate precisely due to the complexity of magnetosphere-disc interactions, we expect λ to lie in the range of 0.1-1, while n_w ranges from somewhat less than unity to a few. Thus both cases and various angle-dependent alignment/misalignment are possible.

In the limit of $L_{\rm d}\gg S$, the evolution equations for $\hat{\boldsymbol{S}}$ and $\hat{\boldsymbol{L}}_{\rm d}$ simplify to

$$\frac{d\hat{\boldsymbol{S}}}{dt}\simeq\omega_0\left(\lambda-\bar{n}_w\cos^2\theta_{\rm sd}\right)\left(\hat{\boldsymbol{L}}_{\rm d}-\cos\theta_{\rm sd}\hat{\boldsymbol{S}}\right) +\left(\Omega_{\rm ps}^{(m)}+\Omega_{\rm ps}\right)\hat{\boldsymbol{L}}_{\rm d}\times\hat{\boldsymbol{S}}, \quad (46)$$

$$\frac{d\,\hat{\boldsymbol{L}}_{\rm d}}{dt}\simeq\Omega_{\rm pd}\,\hat{\boldsymbol{L}}_{\rm b}\times\hat{\boldsymbol{L}}_{\rm d}\qquad({\rm for}\ L_{\rm d}\gg S). \quad (47)$$

We will work in this limit in the following numerical examples.

4.2 Numerical Results

The various accretion/magnetic torques discussed above depend on the parameters $\dot{M}$, λ, $\bar{n}_w$ and $\bar{n}_p$; these are in addition to those parameters that are relevant to the gravitational torques. In general, the accretion rate onto the star, $\dot{M}$, can be smaller than the disc mass depletion rate $|\dot{M}_{\rm d}|$, since the disc may lose mass to outflows/winds or evaporation. In the following examples, for simplicity, we use

$$\dot{M}=|\dot{M}_{\rm d}|=\frac{M_{\rm d0}/\tau}{(1+t/\tau)^2}, \quad (48)$$

and absorb the uncertainty into the parameters λ, $\bar{n}_w$ and $\bar{n}_p$.

Figure 8 shows the results of numerical integration of the spin axis direction for our canonical parameters (with $a_{\rm b}=300$ AU, $\theta_{\rm db}=30^\circ$ and $\theta_{\rm sb}=35^\circ$), with and without accretion/magnetic torques. For $(\lambda,\bar{n}_w,\bar{n}_p)=(1,0.5,1)$, the accretion/magnetic torques, by themselves, tend to damp the spin-disc inclination angle $\theta_{\rm sd}$ since $\lambda-\bar{n}_w\cos^2\theta_{\rm sd}>0$ [see eq. (46)]. In the early stage (see $t\lesssim2.3$ Myrs in the middle panel of Fig. 8), these torques make the spin rotate around $\hat{\boldsymbol{L}}_{\rm b}$ at the same rate as $\hat{\boldsymbol{L}}_{\rm d}$ (see below for discussion). But very quickly the gravitational effect becomes much larger than the accretion/magnetic effects ($|\Omega_{\rm pd}|\gg\omega_0$ for $t\gtrsim1$ Myrs), and $\theta_{\rm sd}$ undergoes large variations. The fact that in the non-adiabatic regime, $\theta_{\rm sb}$ is not as constant as the zero-accretion/magnetic-torque case (compare the middle panel and the upper panel of Fig. 8) may seems surprising, but can be understood pictorially from Fig. 2 and the discussion following equation (44): As $\boldsymbol{S}$ precesses around

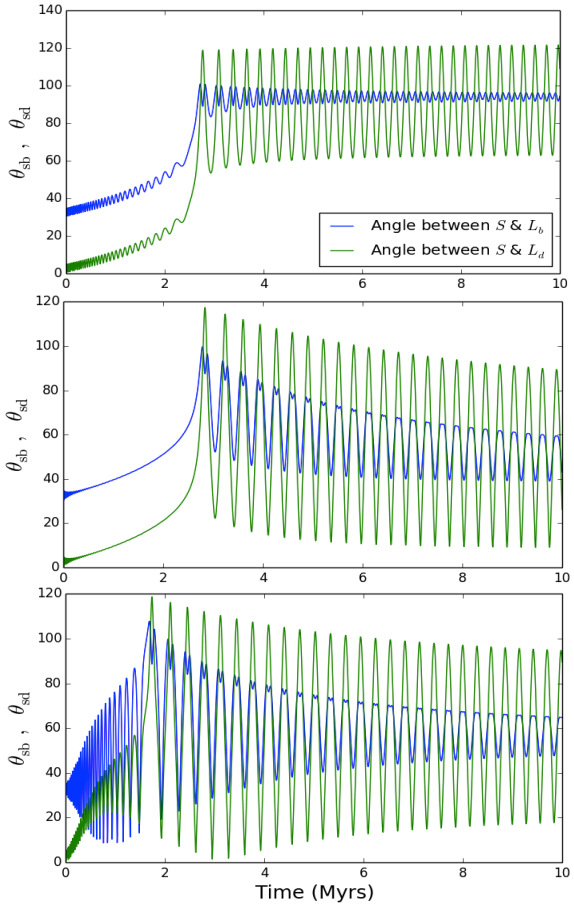

Figure 8. Evolution of the stellar spin direction due to interactions with circumstellar disc and external binary companion, including accretion and magnetic torques. The parameters are the same as in Fig. 4 (i.e., the initial $\theta_{db} = 30^\circ$ and $\theta_{sb} = 35^\circ$, with $a_b = 300$ AU, $\bar{r}_{in} = 1$ and $\bar{\Omega}_\star = 0.1$). The upper panel is for $(\lambda, \bar{n}_w, \bar{n}_p) = (0, 0, 0)$ (i.e., no accretion and magnetic torques), the middle panel $(1, 0.5, 1)$, and the bottom panel $(0.5, 1, 1)$.

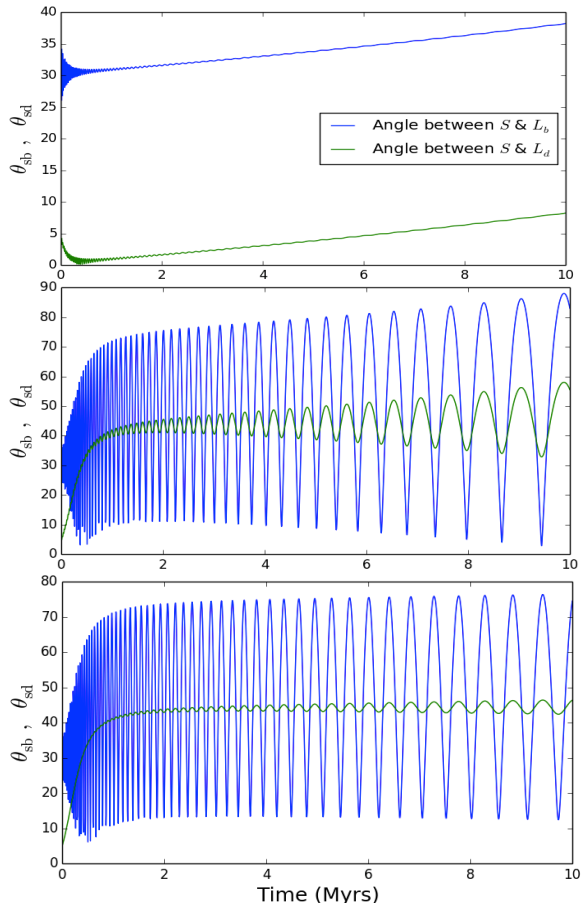

Figure 9. Same as Fig. 8 except for different binary separation a_b. Upper panel: $a_b = 600$ AU, $(\lambda, \bar{n}_w, \bar{n}_p) = (1, 0.5, 1)$; Middle panel: $a_b = 600$ AU, $(\lambda, \bar{n}_w, \bar{n}_p) = (0.5, 1, 1)$; Bottom panel: $a_b = 1000$ AU, $(\lambda, \bar{n}_w, \bar{n}_p) = (0.5, 1, 1)$. The other parameters are the same as in Fig. 8.

$\hat{\boldsymbol{L}}_b$, it is also being pulled toward $\hat{\boldsymbol{L}}_d$, therefore generating variations in θ_{sb} and even larger variations in θ_{sd}.

For $(\lambda, \bar{n}_w, \bar{n}_p) = (0.5, 1, 1)$, the accretion/magnetic torques tend to increase θ_{sd} for small θ_{sd} toward $\theta_{sd+} = 45^\circ$ [see eq. (45)]. This is indeed what happens in the early stage (see the bottom panel of Fig. 8). But soon the gravitational effect takes over and θ_{sd} again exhibits large variations. Again, the qualitative feature of this evolution can be understood from Fig. 2 and the discussion following equation (44).

The situation is somewhat simpler for more distant binary companion (see Fig. 9). Recall that this is the case where the "adiabatic" condition $|\Omega_{ps}/\Omega_{pd}| \gg 1$ is always satisfied (see the lower panel of Fig. 7). For $(\lambda, \bar{n}_w, \bar{n}_p) = (1, 0.5, 1)$, the accretion/magnetic torques alway act to reduce θ_{sd}. For sufficiently large a_b ($\gtrsim 2000$ AU, not shown), we find that θ_{sd} indeed damps and stays close to zero. But for smaller a_b (such as 600 AU; see the top panel of Fig. 9), the damping of θ_{sd} is followed by its gradual growth due to the gravitational effects. This is simply the time-average of behaviour depicted in the lower panel of Fig. 7. For $(\lambda, \bar{n}_w, \bar{n}_p) = (0.5, 1, 1)$ and large a_b (see the bottom panel of Fig. 9), the spin-disc inclination θ_{sd} grows, driven by the magnetic torque, until it saturates at $\theta_{sd+} = 45^\circ$ [eq. (45)], where $\lambda - \bar{n}_w \cos^2\theta_{sd} = 0$. For smaller a_b (such as 600 AU; see the middle panel), θ_{sd} oscillates around 45° due to the gravitational torques.

To understand the behaviour of the θ_{sd} evolution depicted in Fig. 9, we compare in Fig. 10 the precession/rotation of $\hat{\boldsymbol{L}}_d$ and $\hat{\boldsymbol{S}}$ around $\hat{\boldsymbol{L}}_b$. Without the accretion/magnetic torques (see the top panel), we can see that $\hat{\boldsymbol{S}}$ precesses rapidly and follows $\hat{\boldsymbol{L}}_d$ as the latter processes around $\hat{\boldsymbol{L}}_b$ (since $|\Omega_{ps}| \gg |\Omega_{pd}|$). With $(\lambda, \bar{n}_w, \bar{n}_p) = (1, 0.5, 1)$ (see the middle panel), the damping accretion/magnetic torques suppress the precession of $\hat{\boldsymbol{S}}$ around $\hat{\boldsymbol{L}}_d$, making $\hat{\boldsymbol{S}}$ "rigidly" follow $\hat{\boldsymbol{L}}_d$ and precess around $\hat{\boldsymbol{L}}_b$ at rate Ω_{pd}. This explains the smooth, close tracking of θ_{sd} and θ_{sb} (with $\theta_{sb} \simeq \theta_{sd} + 30^\circ$) shown in the top panel of Fig. 9 and the middle panel ($t \lesssim 2.3$ Myrs) of Fig. 8. On the other hand, for $(\lambda, \bar{n}_w, \bar{n}_p) = (0.5, 1, 1)$ (see the bottom panel of Fig. 10), the magnetic torque increases θ_{sd} and makes the rotation of $\hat{\boldsymbol{S}}$ around $\hat{\boldsymbol{L}}_d$ more prominent.

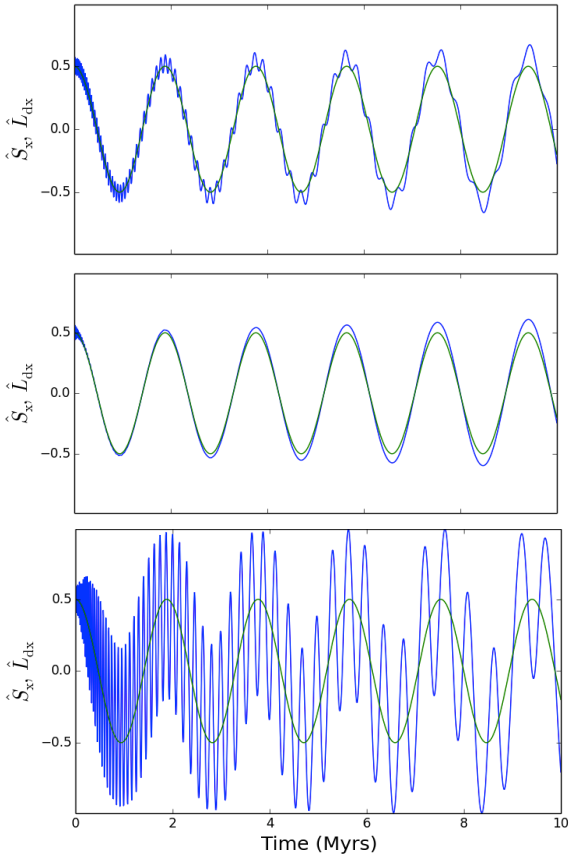

Figure 10. The x-components of $\hat{\boldsymbol{S}}$ (blue lines) and $\hat{\boldsymbol{L}}_{\rm d}$ (green lines) as a function of time for models with $a_{\rm b} = 600$ AU. The z-axis is along $\hat{\boldsymbol{L}}_{\rm b}$. The upper panel is for $(\lambda, \bar{n}_w, \bar{n}_p) = (0, 0, 0)$, the middle panel for $(1, 0.5, 1)$ and the bottom panel for $(0.5, 1, 1)$. The other parameters are the same as in Fig. 8. The corresponding evolutions for $\theta_{\rm sd}$ and $\theta_{\rm sb}$ are shown in Fig. 7 (the lower panel) and Fig. 9 (the upper and middle panels).

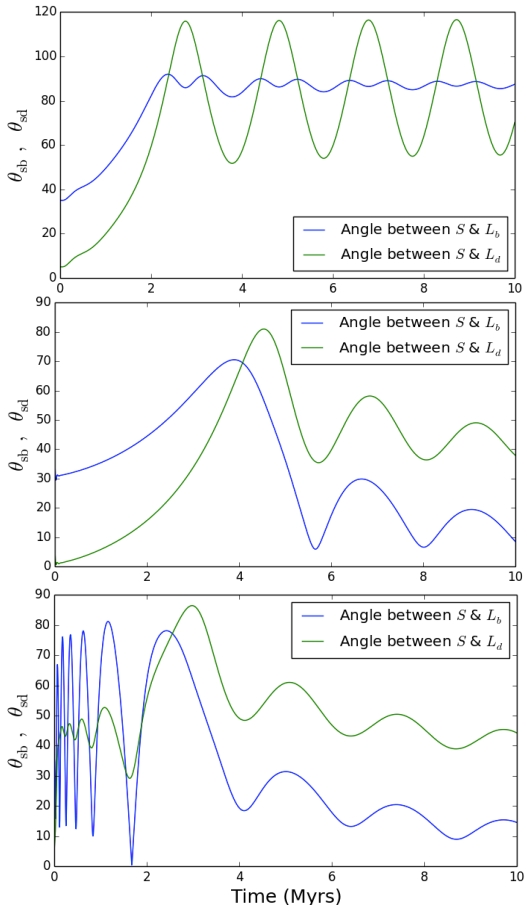

Figure 11. Same as Fig. 8, for $a_{\rm b} = 600$, $\bar{\Omega}_\star = 0.03$ and $r_{\rm in} = 2$. Upper panel: $(\lambda, \bar{n}_w, \bar{n}_p) = (0, 0, 0)$; Middle panel: $(1, 0.5, 1)$; Bottom panel: $(0.5, 1, 1)$. Other parameters are the same as in Fig. 8.

All the examples depicted above assume $\bar{\Omega}_\star = 0.1$ and $r_{\rm in} = 1$. Figure 11 show some cases with a smaller stellar rotation rate, $\bar{\Omega}_\star = 0.03$, with the inner disc radius $r_{\rm in} = 2$, so that the rotation "fastness" parameter is approximately unchanged [see eq. (4)]. This tends to increase the accretion/magnetic effects [see eq. (40)], but also reduce $|\Omega_{\rm ps}|$ [see eq. (14)]. Compare the lower panel of Fig. 7 (for $\bar{\Omega}_\star = 0.1$, $r_{\rm in} = 1$) with the upper panel of Fig. 11, we see that without the accretion/magnetic torques, the reduced $|\Omega_{\rm ps}|$ results is a much larger $\theta_{\rm sd}$, with $\theta_{\rm sb}$ approximately constant at later times. Including the accretion/magnetic torques (the middle and lower panels of Fig. 11), the evolution of spin direction is significantly modified. While some qualitative features of the evolution can be understood from the simple "rules" discussed in Sections 3.1 and 3.3 (see Fig. 2), and the discussion following equation (44), in general it is difficult to "predict" the behaviour of the spin evolution without actual numerical integration of the evolution equations.

5 VISCOUS DAMPING OF DISC INCLINATION

In the preceding sections we have assumed that the disc precesses as a rigid body. In reality, under the tidal forcing of the external companion, the disc is slightly warped. The associated viscous dissipation tends to damp the disc axis relative to the binary axis. Such damping has been estimated or calculated by Bate et al. (2000), Lubow & Ogilvie (2000) and more recently by Foucart & Lai (2014) in the case of small disc warps, based on isotropic α viscosity. The result depends on α and disc thickness, as well as the binary separation. However, the theory adopted in these calculations neglects the potentially important effects of strong, oscillating, shearing flows generated by the warp, which may lead to the development of turbulence (Ogilvie & Latter 2013) and enhance the damping rate. Thus, currently there is significant uncertainty about the damping timescale of disc inclination (see Foucart & Lai 2014 for discussion).

Here to explore the effect of disc inclination damping on the stellar spin evolution, we consider a simple model and assume that the binary-disc angle decays as

$$\theta_{\rm db}(t) = \theta_{\rm db}(0) \exp\left(-t/t_{\rm damp}\right), \qquad (49)$$

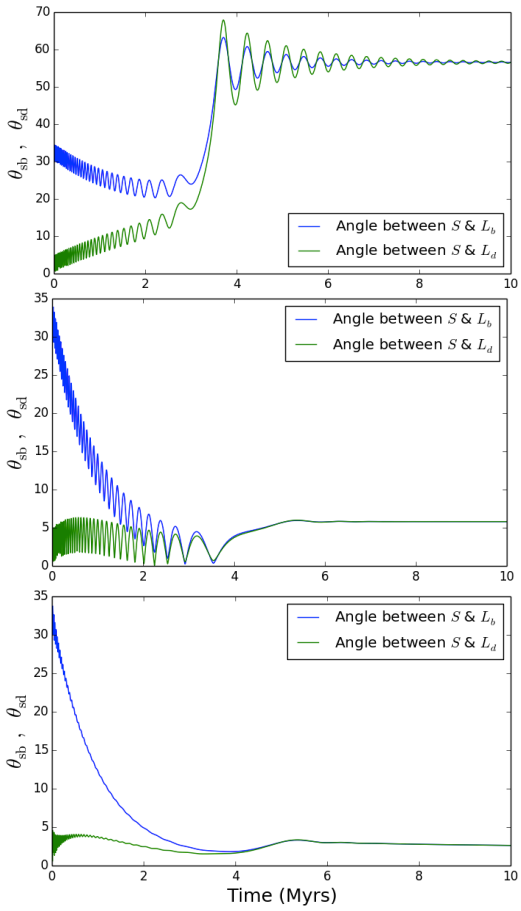

Figure 12. Effect of disc inclination damping on the evolution of stellar spin direction. The system parameters are the same as in Fig. 4, which corresponds to the case with no disc inclination damping ($t_{\rm damp} = \infty$), with $a_{\rm b} = 300$ AU, $\bar{\Omega}_\star = 0.1$, $r_{\rm in} = 1$, initial $\theta_{\rm db} = 30^\circ$, $\theta_{\rm sd} = 5^\circ$ and $\theta_{\rm sb} = 35^\circ$. The upper panel is for $t_{\rm damp} = 2$ Myrs, and the middle panel for $t_{\rm damp} = 0.8$ Myrs; both do not include accretion/magnetic torques. The bottom panel is for $t_{\rm damp} = 1$ Myrs and includes accretion/magnetic torques, with $(\lambda, \bar{n}_w, \bar{n}_p) = (1, 0.5, 1)$.

with $t_{\rm damp}$ a free parameter. Thus, $\hat{\boldsymbol{L}}_{\rm d}$ precesses around $\hat{\boldsymbol{L}}_{\rm b}$ with the frequency $\Omega_{\rm pd}$ but a decreasing $\theta_{\rm db}$.

Figure 12 shows several examples illustrating the effect of disc inclination damping. For the canonical parameters adopted, the damping of $\theta_{\rm db}$ has a significant impact on the final spin direction if $t_{\rm damp}$ is less than a few Myrs. In general, the final spin-disc angle $\theta_{\rm sd}$ is reduced. For $t_{\rm damp} \lesssim 0.8$ Myrs, the final $\theta_{\rm sd}$ is smaller than the initial value (5°). Including the spin-disc damping effect due to accretion/magnetic torques (Section 4) further reduces $\theta_{\rm sd}$.

The examples depected in Fig. 12 (especially the middle and bottom panels) may represent very extreme disc damping rates. They lead to an outcome at the end of disc evolution ($t \sim 10$ Myrs) where the star, disc and binary are all aligned. Such an outcome is inconsistent with observations (such as the spin-orbit misalignments in wide binaries with separations $\gtrsim 40$ AU and the spin-disc misalignments in some young stellar objects; see Section 1). Conceivably, these observations may be used to constrain the physics of dissipation in warped discs.

6 DISCUSSION AND CONCLUSION

In this paper we have examined the idea (Batygin 2012; Batygin & Adams 2013) that the tidal torque on a circumstellar disc from an external binary companion can lead to the generation of misalignment between the disc angular momentum axis and the stellar spin axis. Such "primordial" spin-disc misalignment would contribute to the spin-orbit misalignments observed in many exoplanetary systems containing hot Jupiters. We model the star-disc-binary interactions directly using angular momentum equations, which allow us to describe the secular dynamics of the star-disc-binary system in a simple way and derive the conditions (e.g., disc size, binary separation and stellar rotation rate) under which significant spin-disc misalignments can be produced.

6.1 Key Physical Effects and Results

In general, the tidal torque from the external binary companion makes the circumstellar disc precess around the binary angular momentum axis (at the rate $\Omega_{\rm pd}$) – the disc behaves approximately as a rigid body because the different regions of the disc are coupled by internal waves, viscous stresses or self-gravity. When the disc is misaligned with the rotation axis of the central star, it tends to drive the stellar spin into precession around the disc axis (at the rate $\Omega_{\rm ps}$) due to the rotation-induced oblateness of the star (see Fig. 1). If $|\Omega_{\rm ps}/\Omega_{\rm pd}| \gg 1$, the stellar spin axis $\hat{\boldsymbol{S}}$ will follow the disc axis $\hat{\boldsymbol{L}}_{\rm d}$ adiabatically, so that the spin-disc misalignment angle $\theta_{\rm sd}$ remains approximately constant. However, as the star-disc system evolves in time (e.g., due to decreasing disc mass), $\Omega_{\rm ps}$ decreases [see eq. (14)]. When the ratio $|\Omega_{\rm ps}/\Omega_{\rm pd}|$ crosses unity, significant spin-disc misalignment can be generated. The importance of this secular resonance can be understood in a geometric way (see Fig. 2 and Section 3.4). When $|\Omega_{\rm ps}/\Omega_{\rm pd}| \ll 1$, the stellar spin effectively precesses around the binary axis $\hat{\boldsymbol{L}}_{\rm b}$ with constant spin-binary inclination angle $\theta_{\rm sb}$.

Thus, if the stellar spin and the disc axis are aligned initially, significant spin-disc misalignment can be produced only if the system experiences resonance crossing during its evolution [2]. In the simple disc evolution model considered in this paper (see Sections 2.1 and 3.3), in order to satisfy $|\Omega_{\rm ps}/\Omega_{\rm pd}| \gtrsim 1$ at $t = 0$ (with the initial disc mass $M_{\rm di}$), we require [see eq. (18)]

$$\frac{a_{\rm b}}{r_{\rm out}} \gtrsim 2.8 \left(\frac{M_{\rm b}}{M_\star}\right)^{1/3} \left(\frac{r_{\rm out}}{50\,{\rm AU}}\right)^{-1/6} \left(\frac{\bar{\Omega}_\star}{0.1}\right)^{-7/9} \left(\frac{M_{\rm di}}{0.1 M_\star}\right)^{-1/3}, \quad (50)$$

where $a_{\rm b}$ is the binary separation, $r_{\rm out}$ is the outer disc radius, and we have ignored the non-essential factors on

[2] If the system is in the "non-adiabatic" regime $|\Omega_{\rm ps}/\Omega_{\rm pd}| \ll 1$ at all times, then then $\theta_{\rm sd}$ will simply oscillate between 0° and $2\theta_{\rm db}$, so can periodically attain a large value if $\theta_{\rm db}$ is large (see Fig. 1). However, this is unlike for typical astrophysical star-disc-binary parameters of interest. See equation (50).

the second line of equation (18), and have assumed that $\bar{r}_{\rm in}$ and $\bar{\Omega}_\star$ are related by $f_\star = 0.8$ [see eq. (4)] and thus $(\bar{\Omega}_\star/0.1)\bar{r}_{\rm in}^{-2} = (\bar{\Omega}_\star/0.1)^{7/3}$. On the other hand, to satisfy $|\Omega_{\rm ps}/\Omega_{\rm pd}| \lesssim 1$ at $t = 10$ Myrs (with the "final" disc mass $M_{\rm df}$), we require

$$\frac{a_{\rm b}}{r_{\rm out}} \lesssim 7.6 \left(\frac{M_{\rm b}}{M_\star}\right)^{1/3} \left(\frac{r_{\rm out}}{50\,{\rm AU}}\right)^{-1/6} \left(\frac{\bar{\Omega}_\star}{0.1}\right)^{-7/9} \left(\frac{M_{\rm df}}{0.005 M_\star}\right)^{-1/3}. \quad (51)$$

Thus, in order for produce significant spin-disc misalignment through resonance crossing during the 10 Myrs of the disc lifetime (more precisely when the disc mass changes from $0.1M_\star$ to $0.005M_\star$), the conditions (50)-(51) must be satisfied. Interestingly, most circumstellar disc systems with observed/imaged binary companions have $a_{\rm b}/r_{\rm out}$ in the range between a few to 10 (e.g., Stapelfeldt et al. 1998,2003; Neuhauser et al. 2009; Karl Stapelfeldt, private communication 2013) – such a range is also largely expected from theoretical considerations of the tidal truncation of discs in binaries (e.g., Artymowicz & Lubow 1994). So these conditions can be met in general, although may not always. We note that even when these conditions are not satisfied, $\theta_{\rm sd}$ can still experience modest growth (see, e.g., Fig. 6 and the lower panel of Fig. 7).

Another important aspect of our paper is to incorporate the effects of accretion and magnetic torques in the evolution of the stellar spin direction (Section 4). In general, the magnetic torques between a protostar and its circumstellar disc can induce spin-disc misalignment and contribute to the star-disc mutual precession (Lai et al. 2011), while accretion tends to damp the misalignment. Unfortunately, given the intrinsic complexity of the magnetosphere-disc interaction physics, the net effect accretion and magnetic torques cannot be determined with certainty at present. Nevertheless, we show that these torques in general can influence the evolution of the stellar spin axis in a significant way (see Figs. 8,9,11).

Finally we briefly explore the effect of disc inclination damping (relative to the binary) associated with viscous dissipation of disc warps (Section 5). Only with extreme damping timescales (less than 1 Myrs) can the spin-disc misalignments be significantly affected. By comparing with the observations of spin-orbit misalignments in wide binaries and spin-disc misalignments in protostellar systems, it may be possible to constrain the physics of disc warp dissipations.

6.2 Implications

The general implication of our work is that in the presence of a binary companion, stellar spin-disc misalignments can be generated within the typical lifetimes of protoplanetary discs under a wide range of conditions, as long as the binary axis is somewhat misaligned with the disc axis (by more than a few degrees). There is ample evidence of such disc-binary misalignments from observations of protostellar jets or direct imagings of protostellar discs (see Section 1). In fact, for very reasonable binary/disc parameters, it has proven difficult to avoid the production of significant spin-disc misalignments from small initial values. Although challenging, it would be of great interest to measure or constrain the spin-disc inclination angles of young protostellar disc systems (rather than debris disc systems; see below).

Our general conclusion is consistent with the observations of spin-orbit misalignments in wide ($a_{\rm b} \gtrsim 40$ AU) binaries (Hale 1994). Since there is significant evolution of the spin-disc misalignment angle during the lifetime of the disc, our work suggests that the observed spin-orbit misalignments do not necessarily translate into a large difference in the angular momentum directions of separate molecular cloud cores that form the binary components.

Concerning giant planets, our work suggests that spin-disc misalignments generated by star-disc-binary interactions can make a significant contribution to the observed spin-orbit misalignments in hot Jupiter systems. Such misalignments may already be present prior to any subsequent (after disc dispersal) dynamical processes. Indeed, the same kind of inclined binaries are invoked in the Lidov-Kozai mechanism for producing hot Jupiters (see references in Section 1). Moreover, in order for the Lidov-Kozai migration to operate on a planet at the semi-major axis a_p, the Kozai oscillation period ($\simeq 2\pi/\dot{\omega}_{\rm Kozai}$)

$$P_{\rm Kozai} \simeq 10^6 \left(\frac{a_{\rm b}}{500\,{\rm AU}}\right)^3 \left(\frac{a_p}{5\,{\rm AU}}\right)^{-3} {\rm yrs} \quad (52)$$

must be shorter than the apsidal precession period of the planetary orbit due to general relativity (e.g., Holman et al. 1997). That is, the ratio

$$\frac{\dot{\omega}_{\rm GR}}{\dot{\omega}_{\rm Kozai}} \simeq 6\times 10^{-3} \left(\frac{M_\star}{M_{\rm b}}\right) \left(\frac{a_{\rm b}}{500\,{\rm AU}}\right)^3 \left(\frac{a_p}{5\,{\rm AU}}\right)^{-4} \quad (53)$$

must be less than unity. Thus, if the planet was formed at $a_p \lesssim 1.4$ AU or had migrated (due to disc-driven migration) to such a distance by the end of the protoplanetary disc phase, the binary companion (assuming $a_{\rm b} = 500$ AU) would not be able to induce any Kozai oscillation. Nevertheless, such "failed-Kozai" systems may still have significant spin-orbit misalignments because of the primordial spin-disc misalignments studied in this paper. Of course, whether such systems can have any significant eccentricities or can become hot Jupiters is a different question. In this regard, it is of interest to note that there appears to be a significant lack of super-eccentric proto-hot Jupiters in the Kepler sample (Dawson et al. 2012), suggesting that many hot Jupiters are not produced by high-eccentricity migration mechanism (see Socrates et al. 2012; Dawson & Murray-Clay 2013).

To predict the planet's orbital inclination at the end of the protoplanetary disc phase, it will be necessary to keep track of the evolution of the planet's angular momentum (both magnitude and direction) as the disc evolves and precesses, together with all the other effects considered in this paper. Planet-disc interaction will be an important part of the story (e.g., Baruteau et al. 2013; see also Marzari & Nelson 2009; Terquem 2013; Xiang-Gruess & Papaloizou 2013). Presumably, when the disc is sufficiantly massive as the planet forms and evolves, the angular momentum of the planet will be strongly coupled to that of the disc. If the planet migrates to the close vicinity of the star, the mutual torque between the star and the planet must also be considered. We plan to address some of these issues in the future.

Concerning debris disc systems, current observations do not reveal any evidence of significant spin-disc misalignments (Watson et al. 2011; Greaves et al. 2013; Kennedy et al. 2013). This suggests that the observed/measured sys-

tems, so far, do not have binary companions at all or companions with appropriate separations. Finding binary companions in debris disc systems and measure/constrain the relative orientations of spin, disc and binary axes would be of great interest. On the theoretical side, it would be necessary to extend our study to much later times (beyond 10 Myrs). This would require more reliable models for the evolution of discs from the protoplanetary phase to the debris disc phase.

ACKNOWLEDGMENTS

I thank Diego Munoz for teaching me PYTHON, Kassandra Anderson, Francois Foucart, Diego Munoz and Karl Stapelfeldt for discussions, and Yanqin Wu for comments. This work has been supported in part by NSF grants AST-1008245, AST-1211061 and NASA grant NNX12AF85G.

REFERENCES

Albrecht, S., et al. 2012, ApJ, 757, 18
Albrecht, S., Winn, J.N., et al. 2013, ApJ, 771, 11
Artymowicz, P., Lubow, S.H. 1994, ApJ, 421, 651
Baruteau, C. et al. 2013, arXiv:1312.4293
Bate, M.R., et al. 2000, MNRAS, 317, 773
Bate M.R., Lodato G. & Pringle J.E., 2010, MNRAS, 401, 1505
Batygin, K. 2012, Nature, 491, 418
Batygin, K., Adams, F.C. 2013, ApJ, 778, 169
Bouvier, J., et al. 2007, in Protostars and Planets V, eds. B. Reipurth et al. (Univ. Arizona Press), p.479-494
Chaplin, W.J., et al. 2013, ApJ, 766, 101
Chatterjee, S., et al. 2008, ApJ, 686, 580
Dawson, R.I., Murray-Clay, R.A., Johnson, J.A. 2012, arXiv:1211.0554
Dawson, R.I., & Murray-Clay, R.A. 2013, ApJ, 767, L24
Davis, C.J., Mundt, R., Eisl"offel, J. 1994, ApJ, 437, L58
Fabrycky C. & Tremaine S., 2007, ApJ, 669,1298
Foucart, F., Lai,.D. 2011, MNRAS, 412, 2799
Foucart, F., Lai,.D. 2014, ApJ, to be submitted
Gallet, F., Bouvier, J. 2013, A&A, 556, A36
Ghosh, P., Lamb, F.K. 1979, ApJ, 234, 296
Greaves, J.S., et al. 2013, arXiv:1310.6936
Hale A., 1994, Astron. J., 107, no. 1, p. 306-332
Hebrard, G, et al. 2008, A&A, 488, 763
Hirano, T. et al. 2012, ApJ, 759, L36
Hirano, T. et al. 2014, arXiv:1401.1229
Holman, M.J., Touma, J., Tremaine, S. 1997, Nature, 386, 254
Holman, M.J., et al. 2010, Sci, 330, 51
Huber, D., et al. 2013, Sci, 342, 331
Juric, M., & Tremaine, S. 2008, ApJ, 686, 603
Katz, B., Dong, S., Malhotra, R. 2011, PRL, 107, 181101
Kennedy, G.M., Wyatt, M.C., Bryden, G., Wittenmyer, R., Sibthorpe, B. 2013, MNRAS, 436, 898
Königl, A. 1991, ApJ, 370, L39
Lai, D. 1999, ApJ, 524, 1030
Lai, D. 2014, Theory of disc accretion onto magnetic stars, in "Physics at Magnetospheric Boundary", eds. E. Bozzo et al. (EPJ Web of Conferences, 64, 01001)
Lai, D., Foucart, F. & Lin, D.N.C. 2011, MNRAS, 412, 2790
Lai, D., Rasio, F.A., & Shapiro, S.L. 1993, ApJS, 88, 205
Lai, D., Rasio, F.A., & Shapiro, S.L. 1994, ApJ, 420, 811
Long, M., Romanova, M.M., & Lovelace, R.V.E. 2005, ApJ, 634, 1214
Lubow, S. H. & Ogilvie G. I., 2000, ApJ, 538, 326
Marzari, F., Nelson A.F. 2009, ApJ, 705, 1575
Moutou, C., et al. 2011, A&A, 533, A113
Nagasawa, M., Ida, S., & Bessho, T. 2008, ApJ, 678, 498
Naoz, S. et al, 2011, Nature, 473, 187
Naoz, S., Farr, W.M., Rasio, F.A. 2012, ApJ, 754, L36
Neuhauser et al. 2009 A&A, 496, 777
Ogilvie G.I., 1999, MNRAS, 304, 557
Ogilvie G.I., 2006, MNRAS, 365, 977
Ogilvie, G.I., Latter, H.N. 2013, MNRAS, 433, 2420
Papaloizou J.C.B. & Lin D.N.C., 1995, ApJ, 438, 841
Papaloizou J.C.B. & Pringle J.E., 1983, MNRAS, 202, 1181
Papaloizou, J.C.B., Terquem, C. 1995, MNRAS, 274, 987
Rasio, F.A., & Ford, E.B. 1996, Science, 274, 954
Roccatagliata, V., Ratzka, T., Henning, T., Wolf, S., Leinert, C., & Bouwman, J. 2011, A&A, 534, A33
Rogers, T.M., Lin, D.N.C., Lau, H.H.B. 2012, ApJ, 758, L6
Romanova, M. et al. 2014, in "Physics at Magnetospheric Boundary", eds. E. Bozzo et al. (EPJ Web of Conferences, 64)
Sanchis-Ojeda, R., et al. 2012, Nature, 487, 449
Shu, F.H., et al. 1994, ApJ, 429, 797
Socrates, A., Katz, B., Dong, S., Tremaine, S. 2012, ApJ, 750, 106
Stapelfeldt, K.R., et al. 1998, ApJ, 502, L65
Stapelfeldt, K.R., et al. 2003, ApJ, 589, 410
Terquem, C. 2013, MNRAS, in press (arXiv:1309.1025)
Thies, I., Kroupa, P., Goodwin S.P., Stamatellos, D., Whitworth, A.P. 2011, MNRAS, 417, 1817
Tremaine, S., Davis, S.W. 2013, arXiv:1308.1964
Triaud A. et al., 2010, A&A, 524, A25
Walkowicz, L.M., Basri, G.S. 2013, MNRAS, 436, 1883
Watson, C.A. et al. 2011, MNRAS, 413, L71
Weidenschilling, S.J., & Marzari, F. 1996, Nature, 384, 619
Winn, J.N., et al. 2009, ApJ, 703, L99
Winn, J.N., Fabrycky, D., Albrecht, S., & Johnson, J.A. 2010, ApJ, 718, L145
Wu, Y., & Lithwick, Y. 2011, ApJ, 735, 109
Wu, Y., & Murray, N.W. 2003, ApJ, 589, 605
Wu, Y., Murray, N.W., & Ramshhai, J.M. 2007, ApJ, 670, 820
Xiang-Gruess, M., Papaloizou, J.C.B. 2013, MNRAS, 431, 1336